

Lactobacillus reuteri ZJ617 attenuates metabolic syndrome via microbiota-derived spermidine

Received: 27 March 2023

Accepted: 9 January 2025

Published online: 21 January 2025

 Check for updatesYanfei Ma¹, Yifan Zhong¹, Wenjie Tang¹, Teresa G. Valencak¹, Jingliang Liu¹, Zhaoxi Deng¹, Jiangdi Mao¹, Daren Liu², Shanshan Wang¹, Yuhao Wang³✉ & Haifeng Wang¹✉

Metabolic syndrome (MetS) is a difficult-to-manage disease that poses a significant risk to human health. Here, we show that the supplementation of *Lactobacillus reuteri* ZJ617 ameliorates symptoms of MetS in mice induced by the high-fat diet. *L. reuteri* ZJ617 modulates host metabolism by interacting with the microbiome, resulting in the production of spermidine synthesized by the microbiota. *L. reuteri* ZJ617 serves as a source of substrates for the microbiota to synthesize spermidine, hence preventing the decline of bacteria responsible for spermidine production. Spermidine treatment mimics the metabolic effects of *L. reuteri* ZJ617, whereas pharmacological inhibition of spermidine biosynthesis in mice abolishes these benefits. Our findings reveal the mechanism by which *L. reuteri* ZJ617 alleviates MetS symptoms and provide support for its potential use as a probiotic for promoting metabolic health.

The metabolic syndrome (MetS) is a prevalent global health issue. If left untreated, MetS may lead to deleterious metabolic illnesses, including obesity, type 2 diabetes mellitus (T2D), and nonalcoholic fatty liver disease (NAFLD)^{1,2}. In mammals, adipose tissue is an active endocrine metabolic organ involving whole-body energy homeostasis³. Individuals with an excess of intra-abdominal or visceral adipose tissue are at substantially higher risk of being diagnosed with MetS⁴. Although white adipose tissue (WAT) acts to store energy, brown adipose tissue (BAT), which is limited in adult humans^{5,6}, plays a crucial role in energy expenditure⁷. Therefore, transforming white to brown-like adipocytes are a promising strategy for treating metabolic disorders.

Lactobacillus species have a long history of safe use in food and have been proven to improve host metabolic health⁸. Shotgun metagenomic sequencing has revealed a positive correlation between *L. reuteri* in feces and reduced adiposity⁹. Multiple randomized clinical trials have reported an inverse relationship between the consumption of *L. reuteri* and the incidence of MetS^{10–12}. A prior study also demonstrated an anti-obesity effect of *L. reuteri*, which appears to be

associated with the remodeling of WAT and energy metabolism¹³. However, the molecular mechanism underlying the metabolic benefits of *L. reuteri* requires further clarification.

In the intestine, trillions of commensal bacteria produce a variety of bioactive metabolites and play essential roles in metabolism¹⁴. These metabolites, including short-chain fatty acids, bile acids, branched-chain amino acids, indole derivatives, and endocannabinoids, can reprogram energy expenditure by affecting non-shivering thermogenesis in adipose tissue^{15,16}. Given that a recent study revealed a close link between the metabolic regulatory ability of *Lactobacillus* and the intestinal microbiota¹⁷, it is possible that *L. reuteri* delivers metabolic benefits to the host by promoting the production of certain metabolites from the microbiota. Thus, the goal of the present study was to gain a deeper understanding of the beneficial effects of *L. reuteri* in relation to metabolic syndrome and to determine the potential role of gut microbiota and their metabolites in achieving these benefits.

Our previous studies have demonstrated that dietary supplementation with *L. reuteri* ZJ617 improves the health of the intestine and liver^{18–20}. The present study further revealed that *L. reuteri* ZJ617

¹The Key Laboratory of Molecular Animal Nutrition, Ministry of Education, College of Animal Sciences, Zhejiang University, Hangzhou, Zhejiang 310058, PR China. ²The Second Affiliated Hospital of Zhejiang University, Hangzhou, Zhejiang 310009, PR China. ³Institute of Translational Medicine, Zhejiang University School of Medicine, Hangzhou, Zhejiang 310029, PR China. ✉e-mail: yuhao.wang@zju.edu.cn; haifeng.wang@zju.edu.cn

alleviates MetS and promotes the transforming of white to brown-like adipose tissue in mice fed with a high-fat diet (HFD). Mechanistically, *L. reuteri* ZJ617 provides substrates to spermidine-producing bacteria, promoting the production of spermidine and preserving sufficient levels of spermidine in circulation and WAT. Spermidine supplementation delivers similar metabolic benefits to *L. reuteri* ZJ617, while pharmaceutical inhibition of spermidine biosynthesis abolished these benefits. Our findings highlight the significance of spermidine as a microbiota-derived molecule that contributes to the metabolic benefits of *L. reuteri* and further supports the use of *L. reuteri* as a probiotic to treat MetS.

Results

L. reuteri ZJ617 alleviates the symptoms of metabolic syndrome in HFD-fed mice

In order to evaluate the effects of *L. reuteri* ZJ617 on MetS, we chose HFD-fed mice as the model (Fig. 1a). As expected, the mice fed the HFD for 14 weeks developed obesity (Fig. 1b, c) and exhibited reduced oxygen consumption, CO₂ production, and energy expenditure in both light and dark (Supplementary Fig. 1a, b) in comparison to the control group of mice fed a low-fat diet (LFD). However, supplementing HFD-fed mice with *L. reuteri* ZJ617 effectively reduced body weight gain (Fig. 1b, c), improved oxygen consumption, CO₂ production, energy expenditure (Fig. 1d and Supplementary Fig. 1c), and reversed the decrease of rectal temperature caused by HFD (Fig. 1e). In addition, *L. reuteri* ZJ617 supplementation in HFD-fed mice effectively reduced the concentrations of serum triglycerides (TG), total cholesterol (TC) and low-density lipoprotein cholesterol (LDL-C) (Supplementary Fig. 1d–f), and efficiently improved glucose tolerance and insulin sensitivity (Fig. 1f, g). The homeostasis model assessment of insulin resistance (HOMA-IR) score further revealed that *L. reuteri* ZJ617 supplementation was able to attenuate the severity of insulin resistance caused by HFD (Fig. 1h). Importantly, the comparable liver weight, alleviated hepatic steatosis (Supplementary Fig. 1g–i), and improved liver function (Supplementary Fig. 1j, k) demonstrate that long-term oral administration of *L. reuteri* ZJ617 had limited side effects. Of note, there was no significant difference in food intake between mice supplemented with *L. reuteri* ZJ617 and mice fed with only HFD (Supplementary Fig. 1l, m), suggesting that the metabolic benefits of *L. reuteri* ZJ617 were not due to a decrease in food consumption.

Remarkably, detailed tissue analysis showed that mice supplemented with *L. reuteri* ZJ617 had significantly fewer adipose depots and smaller lipid droplets in adipocytes than mice fed with only HFD (Fig. 1i–k). Transmission electron microscopy (TEM) showed a higher density of mitochondria (Fig. 1l and Supplementary Fig. 1n) and higher expression of mitochondrial biogenesis genes (*Cox5b*, *Cox7a1*, *Cox7a2*) (Fig. 1n) in epididymis adipose tissue (e-WAT) from mice supplemented with *L. reuteri* ZJ617 compared to mice fed with only HFD. Proteins (UCP1 and ADRB3) (Fig. 1m) and mRNAs (*Adrb3*, *Pgc-1b*, *Pparg*, and *Pparg*) (Fig. 1n) relevant to the browning process were also upregulated in e-WAT in mice supplemented with *L. reuteri* ZJ617 compared to mice fed with only HFD, despite a decrease in the mRNA level of *Ucp1* gene (Supplementary Fig. 1o). Together, our results indicate that *L. reuteri* ZJ617 treatment mitigates MetS and may activate the browning process of WAT in HFD-fed mice.

L. reuteri ZJ617 modulates gut microbiota in HFD-fed mice

Previous study has suggested that the improvement of host metabolism by single bacteria or bacterial consortia does not rule out the possibility of microbe-microbe interactions²¹. We thus investigated the impacts of *L. reuteri* ZJ617 on the gut microbiota by performing 16S ribosomal RNA gene amplicon sequencing on intestinal contents from HFD-fed mice supplemented with or without *L. reuteri* ZJ617 and LFD-fed mice. The unweighted UniFrac-based principal coordinates

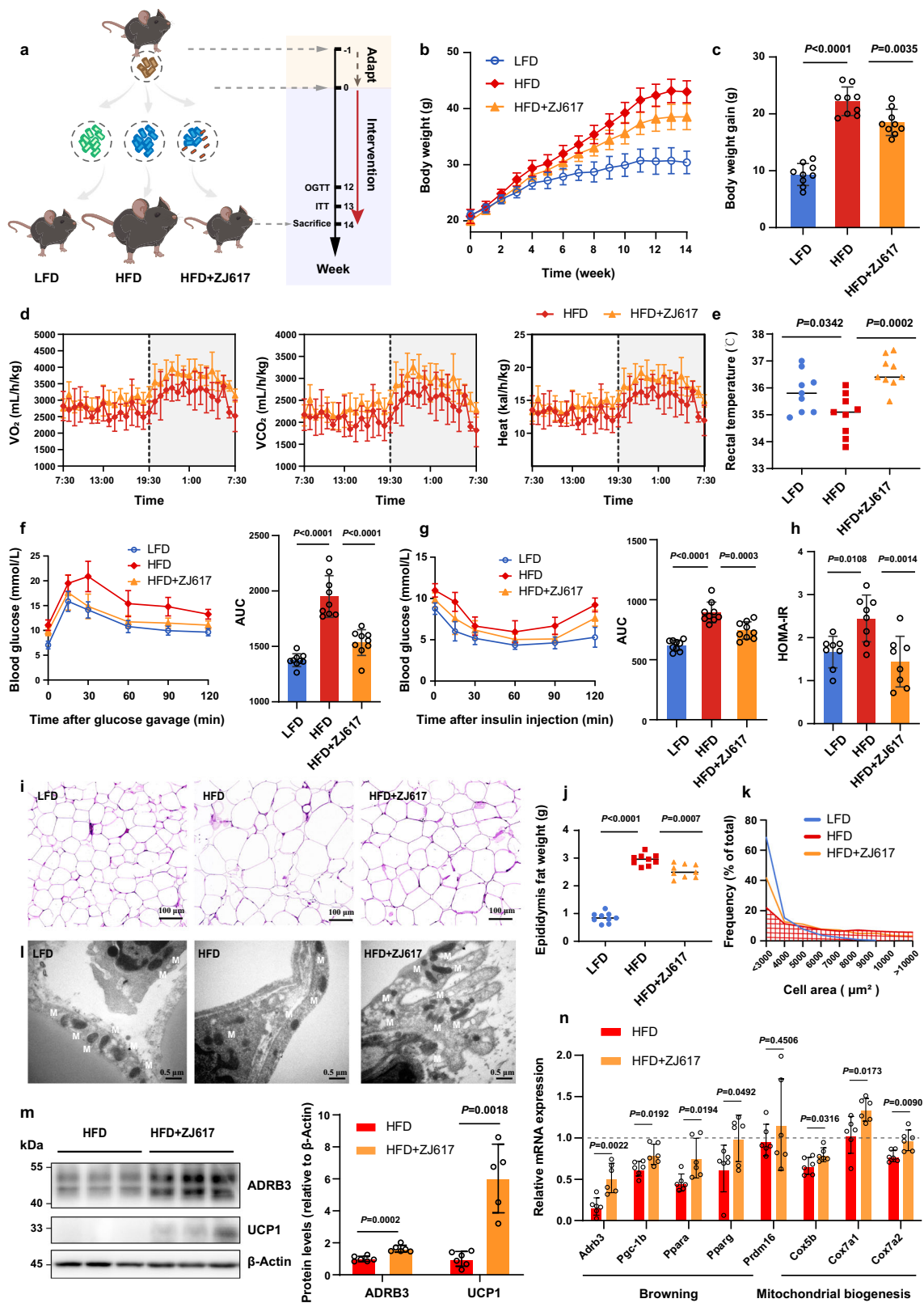
analysis (PCoA) revealed a clear clustering of the gut microbiota for each group (Fig. 2a). *L. reuteri* ZJ617 supplementation resulted in a shift in β -diversity (Fig. 2b) and a reversal of the Firmicutes-to-Bacteroidetes ratio ($P = 0.07$) (Fig. 2c, d) in comparison to mice fed with only HFD. A random forest classifier was applied to further identify the specific microbiota that was altered by the *L. reuteri* ZJ617 treatment ($P < 0.1$). Overall, out of 409 amplicon sequence variants (ASVs), 100 ASVs showed different relative abundances between LFD-fed and HFD-fed mice (Supplementary Fig. 2), and *L. reuteri* ZJ617 supplementation affected 45 ASVs, with 20 enriched and 25 reduced when compared to HFD-fed mice (Fig. 2e). At the genus level, HFD feeding led to decreased abundances of *Parabacteroides*, *Roseburia*, *Bacteroides*, *Muribaculaceae* and *Parasutterella* compared to mice fed an LFD (Supplementary Fig. 2), while *L. reuteri* ZJ617 supplementation prevented this decline (Fig. 2e). Moreover, *L. reuteri* ZJ617 supplementation increased the fecal abundance of *Lactobacillus* at different time points in comparison to mice fed with only HFD (Supplementary Fig. 1p).

To further understand the functional potential of these reorganized microbial communities, PICRUSt2 was applied to predict metagenome functions. Among the 355 identified pathways, 64 exhibited differential abundance in the intestinal contents of mice supplemented with *L. reuteri* ZJ617 compared to the HFD-fed mice ($P < 0.05$). Pathways related to polyamine synthesis were among the top-ranked upregulated pathways (Fig. 3a), and higher levels of the key genes responsible for polyamine production (Fig. 3b) and transportation (Fig. 3c) were detected. Although amplicon-based prediction was unable to distinguish strain-specific functionality due to insufficient resolution, the BlastP analysis (bit score >200) validated the presence of key genes involved in polyamine synthesis in the bacteria genus upregulated by *L. reuteri* ZJ617 (Fig. 3d, e). This result is consistent with previous studies showing spermidine production capacity in *Parabacteroides*, *Roseburia*, and *Bacteroides*^{22,23}. Thus, our findings indicate that supplementation of *L. reuteri* ZJ617 reshapes the composition and function of the microbiota in HFD-fed mice, which may lead to upregulation of key microbial genes involved in polyamine biosynthesis.

The metabolic benefits of *L. reuteri* ZJ617 are mediated by the gut microbiota

In order to investigate whether the *L. reuteri* ZJ617-induced microbial shift directly contributes to metabolic protection, we transplanted fecal microbiota from three experimental groups separately into recipient mice that had been pre-treated with antibiotic mixtures to remove microbiota. The recipient mice were then maintained on HFD for 14 weeks (Fig. 4a). Mice transplanted with HFD microbiota (FHH) showed a marked increase in body weight gain compared to mice transplanted with LFD microbiota (FLH), whereas mice transplanted with HFD + ZJ617 microbiota (FZH) exhibited a significant reduction in weight gain compared to FHH mice (Fig. 4b, c). In addition, compared to FHH mice, FZH mice showed an enhanced ability to clear blood lipids (Supplementary Fig. 3a–c), improved glucose tolerance and insulin sensitivity (Fig. 4d, e), healthier serum AST and ALT levels (Supplementary Fig. 3d, e), and reduced accumulation of adipose depots and adipocyte areas (Fig. 4f–h). There was no significant difference in liver weights or hepatic triglyceride levels between FHH and FZH mice (Supplementary Fig. 3f–h). Notably, FZH mice exhibited similar WAT browning as observed in the donor mice. The mitochondrial density (Fig. 4i and Supplementary Fig. 3i) and the expression of “browning” associated marker proteins (ADRB3 and UCP1) (Fig. 4j) and genes (*Adrb3*, *Pgc-1b*, *Pparg* and *Cidea*) (Fig. 4k) were all upregulated in WAT of FZH mice as compared to FHH mice.

We then conducted 16S rRNA sequencing to examine the composition of the intestinal microbiota in the recipient mice. The PCoA analysis revealed a compositional difference between the microbiota of FHH mice and FZH mice (Supplementary Fig. 4a, b). The heatmap



showed that 71 ASVs were changed in FZH mice and 90 ASVs were changed in FLH mice (Supplementary Fig. 4c, d). Compared to FHH mice, the abundances of *Parabacteroides* and *Muribaculaceae* were significantly higher in FZH mice, but there was no significant difference for *Parasutterella*, *Roseburia*, and *Bacteroides* (Supplementary Fig. 4d). Consistent with HFD-fed mice supplemented with *L. reuteri* ZJ617, the prediction of metagenome functions indicated that the pathways

related to polyamine biosynthesis were more abundant in FZH mice than in FHH mice (Supplementary Fig. 5a). The key genes and transport proteins involved in polyamine production were also enriched in the FZH mice compared to the FHH mice (Supplementary Fig. 5b, c). Together, these results indicate that there exists a causal relationship between microbiota-related polyamine synthesis and the metabolic benefits of *L. reuteri* ZJ617.

Fig. 1 | *L. reuteri* ZJ617 alleviates the feature of metabolic syndrome in HFD-fed mice. **a** Study design of *L. reuteri* ZJ617 intervention experiment. Mice were randomly assigned to three groups ($n = 9$ per group). LFD-fed mice were provided with fresh drinking water on a daily basis. High-fat diet (HFD)-fed mice were treated with fresh drinking water or *L. reuteri* ZJ617 (10^9 CFU/mL) in drinking water for 14 weeks. The drinking water was refreshed every day. The figure is drawn by Adobe Illustrator CC 2018. **b** Body weights were measured throughout the 14 weeks period and the end of the experiment (c) body weight gain was calculated. **d** Effect of *L. reuteri* ZJ617 administration on energy metabolism, including oxygen consumption, CO₂, and heat production assessed after 4 weeks of intervention. **e** Rectal temperatures from all three groups of mice. The effects of *L. reuteri* ZJ617 on glucose tolerance measured by (f) oral glucose tolerance test (OGTT). Right: Area

under the curve (AUC). The effects of *L. reuteri* ZJ617 on insulin tolerance measured by (g) insulin tolerance test (ITT). Right: Area under the curve (AUC). **h** HOMA-IR was calculated by fasting blood glucose (mmol/L) \times fasting insulin (mIU/L)/22.5. **i** Representative H&E picture of WAT (scale bars, 100 μ m). **j** WAT weight. **k** Frequency distribution of adipocyte cell sizes. **l** Representative TEM images of e-WAT (scale bars, 0.5 μ m). **m** Protein levels of ADRB3 and UCP1 in WAT ($n = 6$ per group). **n** mRNA levels of non-shivering thermogenesis-related genes relative to *Gapdh* in WAT ($n = 6$ per group). LFD group served as a reference and is represented by a dashed line. Data were shown as mean \pm SD. Significances in all panels are calculated based on one-way ANOVA with Dunnett tests for multiple-group comparisons, with the exception of (m, n) calculated based on two-tailed *t*-tests. Source data are provided as a Source Data file.

L. reuteri ZJ617 supplementation increases the production of microbiota-derived spermidine

We next performed untargeted metabolomic profiling on intestinal contents to identify potential microbial molecules communicating between the host and the microbiome. A total of 530 metabolites were detected in the intestinal contents. The orthogonal partial least squares-discrimination analysis (OPLS-DA) showed distinct clustering of metabolites among LFD-fed mice, HFD-fed mice, and HFD-fed mice supplemented with *L. reuteri* ZJ617 (Fig. 5a). Compared to LFD-fed mice, HFD-fed mice exhibited an increase of 52 metabolites and a decrease of 27 metabolites (Supplementary Table 3). *L. reuteri* ZJ617 supplementation resulted in the upregulation of 8 metabolites and the downregulation of 15 metabolites in HFD-fed mice (Fig. 5b and Supplementary Table 4). The pathway enrichment analysis showed that *L. reuteri* ZJ617 supplementation had the most significant impact on the arginine and proline metabolism pathway (Fig. 5c), which is involved in polyamine production. In agreement with the prediction of the metagenome functions, spermidine levels were increased after *L. reuteri* ZJ617 supplementation (Fig. 5b). We then performed targeted polyamine metabolomics on both intestinal contents and serum samples to validate the results. For intestinal contents, most of the metabolites on polyamine metabolism (L-Arginine, Agmatine, S-adenosylmethionine, L-Ornithine, Spermidine) were significantly higher in mice supplemented with *L. reuteri* ZJ617 than in mice fed with only HFD. Furthermore, supplementation of *L. reuteri* ZJ617 only increase the concentration of spermidine in serum (Fig. 5d), while the level of spermine was significantly reduced (Fig. 5d). The levels of spermidine were consistently found to be higher in both the intestinal contents and serum of FZH mice than in FHH mice (Supplementary Fig. 6a, b).

Previous research has established that spermidine is obtained orally through dietary sources, such as the polyamine precursor arginine, or through the synthesis by commensal bacteria²⁴. Whether spermidine was produced by *L. reuteri* ZJ617 or by commensal gut bacteria remains unknown in our setting. The genomic information revealed that *L. reuteri* ZJ617 only expresses genes that encode spermidine/putrescine transport proteins (Supplementary Table 5), but not genes that are essential for spermidine synthesis. Therefore, we detected a decrease of spermidine in the supernatant of cultured *L. reuteri* ZJ617 (Supplementary Fig. 6d). Notably, we found that *metK* gene, that encode S-adenosylmethionine synthetase, is expressed by *L. reuteri* ZJ617 (Supplementary Table 5). This aligns with the observation of increased S-adenosylmethionine (SAM) levels in the intestinal contents of mice supplemented with *L. reuteri* ZJ617 (Fig. 5d), as well as in the intestinal contents of FZH mice (Supplementary Fig. 6c). The in vitro cultivation of *L. reuteri* ZJ617 revealed additional evidence supporting the production of SAM by *L. reuteri* ZJ617 (Fig. 5e). Because SAM is the precursor of spermidine, our findings suggest that *L. reuteri* ZJ617 is able to provide substrates for other spermidine-producing bacteria.

To better understand the efficacy of *L. reuteri* ZJ617 in facilitating the production of microbiota-derived spermidine, we applied a

gastrointestinal tract simulation system to examine the SAM levels in the simulated gut lumen that was inoculated with fecal microbiota from individuals with obesity (Fig. 5f). Consistent with the results obtained from mice metabolomics (Fig. 5d), SAM levels were observed to be higher if *L. reuteri* ZJ617 was co-cultured in the simulated gut lumen (Fig. 5g). As the same time, both the abundance of spermidine-producing bacteria and the level of spermidine increased in the simulated gut lumen co-cultured with *L. reuteri* ZJ617 in vitro (Supplementary Fig. 6e–g and Fig. 5h). Importantly, the addition of SAM to the simulated gut lumen also increases the abundance of spermidine-producing bacteria and the production of spermidine (Supplementary Fig. 6e–g and Fig. 5h). Although the BlastP analysis (Fig. 3d) and previous studies have demonstrated the spermidine production capacity of *Parabacteroides*, *Roseburia*, and *Bacteroides*^{22,23}, in this study, *Bacteroides* was reconfirmed to have ability to convert SAM into spermidine in in vitro cultivation. Spermidine level in the supernatant significantly increased after co-culturing *Bacteroides* with SAM, compared with the supernatant containing only SAM. (Supplementary Fig. 6h). These findings collectively suggest that *L. reuteri* ZJ617 promotes spermidine production in fecal bacteria from individuals with obesity.

Microbiota-derived spermidine ameliorates metabolic syndrome and promotes the browning of WAT

To further assess the importance of spermidine biosynthesis in mediating the metabolic benefits of *L. reuteri* ZJ617, we added spermidine directly into the drinking water of mice given an HFD (Fig. 6a). Compared to mice fed with only HFD, spermidine supplementation markedly lowered body weights (Fig. 6b, c), improved hyperlipidemia and insulin tolerance (Fig. 6d, e, h), reduced liver weights and triglycerides (Fig. 6i, j), and alleviated hepatic steatosis (Fig. 6k), although did not improve LDL-C levels and glucose tolerance (Fig. 6f, g). Importantly, spermidine supplementation also promoted energy metabolism (Supplementary Fig. 7a–c), elevated WAT temperature (Fig. 7a, b), reduced WAT accumulation and adipocyte areas (Fig. 7c–e), augmented mitochondria density (Fig. 7f and Supplementary Fig. 7d), and upregulated the expression of mitochondrial biogenesis genes (*Cox5b*, *Cox7a1*, *Cox7a2*) (Fig. 7h), browning-related proteins (ADRB3 and UCP1) (Fig. 7g) and mRNAs (*Adrb3*, *Ppara*, and *Pparg*) (Fig. 7h).

As a comparison, we administered a polyamine biosynthesis pathway inhibitor, diminazene aceturate (DA) to mice via gavage. DA has been found to hinder the formation of S-adenosylmethionine^{25,26}, and block the activity of spermidine/spermine N1-acetyltransferase, hence inhibiting the back conversion of spermidine and spermine into putrescine^{27,28}. Therefore, DA could cut off both putrescine and S-adenosylmethionine-derived polyamine synthesis pathways. We found that DA administration through intraperitoneal injection or oral gavage had no effect on spermidine levels in WAT of mice fed with either a normal diet or HFD (Supplementary Fig. 7e, f), but it significantly decreased spermidine level in intestinal contents from HFD-fed mice (Supplementary Fig. 7g). These results indicate that the

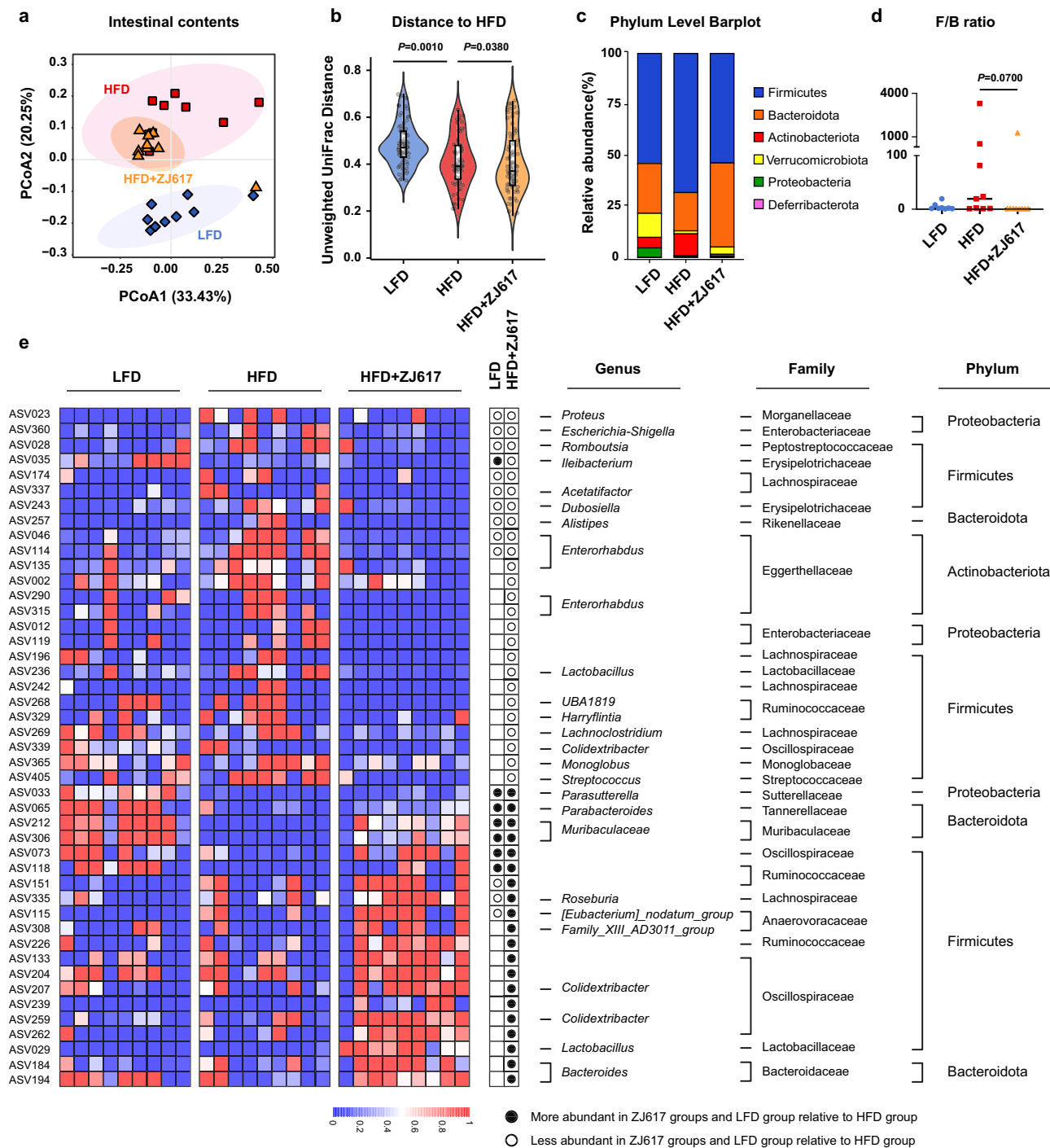


Fig. 2 | *L. reuteri* ZJ617 re-programs gut microbiota composition of HFD-fed mice. Microbiota composition of LFD, HFD, and HFD + ZJ617 was analyzed by 16S rDNA ($n = 9$ per group). **a** Unweighted UniFrac PCoA analysis of gut microbiota. **b** Unweighted UniFrac distance of gut microbiota. **c** Phylum taxonomic level. **d** Firmicutes to Bacteroidetes (F/B) ratio. **e** The changing direction of the 45 ASVs by *L. reuteri* ZJ617 according to random forests classifier. Circles represent less abundant ASVs in LFD and *L. reuteri* ZJ617 relative to the HFD group; Black dots

indicate higher abundances of ASVs in LFD and *L. reuteri* ZJ617 relative to the HFD group. The taxonomy of the ASVs (genus, family, and phylum) are shown on the right. The box plots shown as minima, maxima, center, bounds of box and whiskers, and percentile. Significance in (b) is calculated based on two-tailed PERMANOVA with pseudo- F tests. Data in (d) are shown as mean \pm SD, and significance is calculated based on one-way ANOVA with Kruskal–Wallis tests for multiple-group comparisons.

dosage of DA we used can reduce spermidine synthesis by the gut microbiota while having a minor impact on spermidine production in adipose tissue. Remarkably, when DA was administered to HFD-fed mice supplemented with *L. reuteri* ZJ617, the metabolic benefits of *L. reuteri* ZJ617 were largely abolished (Fig. 6b–k), and the non-shivering thermogenesis in WAT was also decreased (Fig. 7a–h).

Since spermidine reaches target tissues through rapid plasma turnover to exert physiological functions²⁹, we measured spermidine concentrations in WAT from HFD-fed mice that underwent different treatments. As compared to control mice given only an HFD, oral administration of spermidine significantly increased spermidine levels in WAT, with an increasing trend observed for *L. reuteri* ZJ617

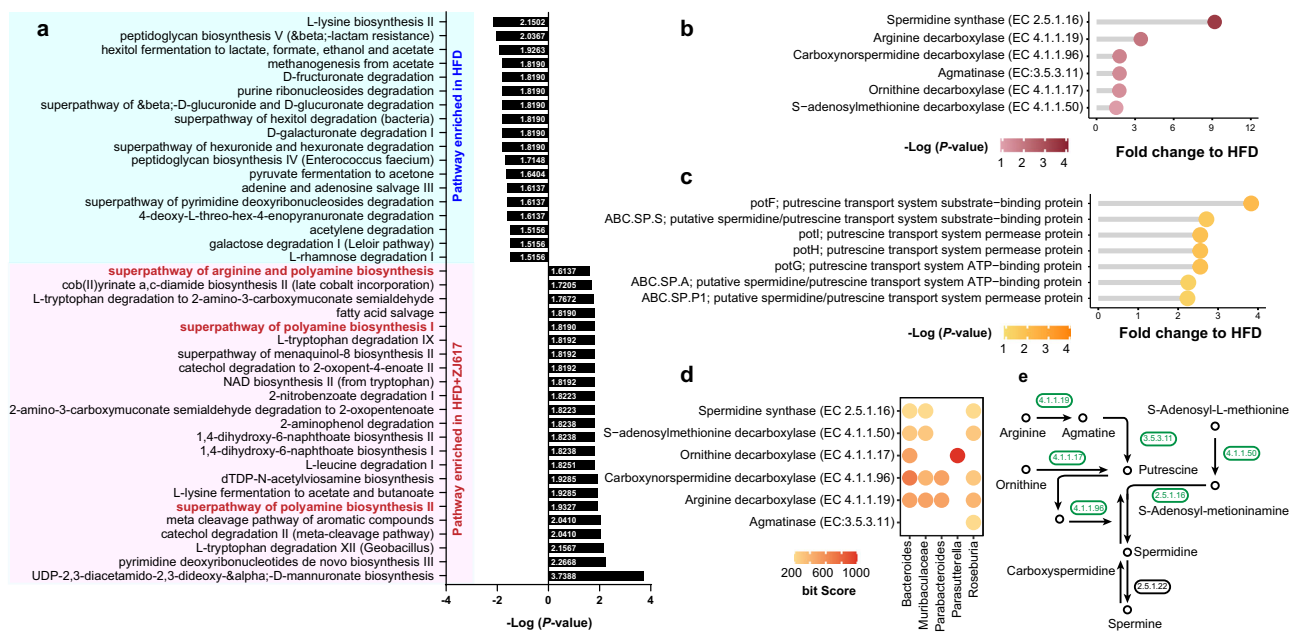


Fig. 3 | *L. reuteri* ZJ617 changes microbial function of HFD-fed mice. a Bar chart represents functional pathways in intestinal contents predicted using PICRUST2. The pathways enriched in *L. reuteri* ZJ617 are marked as red panels, and pathways enriched in HFD are marked as blue panels. The polyamine pathways are marked with red fonts. **b** The key enzymes involved in polyamine biosynthesis. **c** The prediction of polyamine transport system. **d** Occurrence of homologous proteins responsible for polyamine synthesis upregulated by *L. reuteri* ZJ617 in the gut microbiota by BlastP

analysis. **e** Graphical representation of the polyamine biosynthetic pathway. The enzymes marked as green-colored indicated an increase in *L. reuteri* ZJ617-treated mice, and black-colored symbols indicated no significant changes. 4.1.1.19, arginine decarboxylase; 4.1.1.17, ornithine decarboxylase; 3.5.3.11, agmatinase; 4.1.1.96, coxynorspermidine decarboxylase; 4.1.1.50, S-adenosylmethionine decarboxylase; 2.5.1.16, spermidine synthase. 2.5.1.22 spermine synthase. Significance is calculated using two-tailed Wilcoxon tests ($n = 9$ per group).

($P = 0.08$). However, there was no significant difference for HFD-fed mice given *L. reuteri* ZJ617 in combination with DA (Fig. 7i). Similarly, FZH mice showed an increased spermidine level in WAT as compared to FHH mice (Supplementary Fig. 7h).

In order to further confirm a direct involvement of spermidine in adipocyte browning, we treated the preadipocyte cell line 3T3-L1 with spermidine during its chemical-induced differentiation. The addition of spermidine resulted in a significant reduction in lipid droplets (Fig. 7j and Supplementary Fig. 7i) and an increase in the levels of adipocyte browning-related proteins (ADRB3 and UCP1) (Fig. 7k). Together, our data provide mechanistic evidence that spermidine acts as a potential molecule that mediates the metabolic benefits of the *L. reuteri* ZJ617 in improving MetS and promoting adipocyte browning.

Discussion

There is strong evidence from randomized clinical trials and meta-analyses that the administration of *L. reuteri* is associated with a lower risk of MetS^{10–12,30}. In this study, we showed that intake of *L. reuteri* ZJ617 improves MetS in HFD-induced obese mice. We found no clear adverse effects in mice following long-term *L. reuteri* ZJ617 exposure, as we had seen in our prior study in pig and mouse models fed a normal diet^{18,31}. We discovered that *L. reuteri* ZJ617 impacts the composition and function of the gut microbiome while offering metabolic benefits to the host. *L. reuteri* ZJ617 modulates energy metabolism, promotes WAT browning, and mitigates MetS symptoms by providing substrates for the microbiota to synthesize microbial-derived spermidine.

Although multiple studies have reported *L. reuteri* supplementation can modulate gut microbiota of mouse models and humans with metabolic disorders^{11,32,33}, few studies have focused on the modulation of host metabolism by specific microbial metabolites derived from *L. reuteri* or *L. reuteri*-modulated commensal bacteria. In this study, we discovered that microbial-derived spermidine is the major contributor to the metabolic benefits of *L. reuteri* ZJ617, and that *L. reuteri* ZJ617 can

provide a substrate for commensal bacteria to synthesize spermidine. Because the *metK* gene has been identified in various *Lactobacillus* species in another study³⁴, our study indicates that spermidine synthesis via reciprocity may be a key reason for the probiotic effects of numerous *Lactobacilli*.

A growing body of literature supports the role of spermidine in modulating host metabolism. One study has found that daily intake of spermidine was negatively correlated with body mass index (BMI), waist circumference, and HOMA-IR index in humans³⁵. The mechanism by which spermidine exerts its metabolic benefits including gut barrier enhancement³⁵, hepatic mitochondrial function improvement³⁶, BAT activation, and muscle adaptation³⁷. However, few studies have shown that spermidine impacts on WAT. Since excess WAT accumulation is a major risk factor for developing MetS³⁸, activating WAT browning is critical for improving human health. Herein, we found that both *L. reuteri* ZJ617 and spermidine improve whole-body energy metabolism and promote WAT browning. A previous study has confirmed that spermidine promotes WAT lipolysis in an ADRBs-dependent way³⁹. Spermidine mimics the β -adrenergic stimulation activating ADRBs receptor, thereby increasing cyclic AMP levels, and driving protein kinase (PKA) signaling to promote lipolysis³⁹. These released fatty acids via adipocyte lipolysis subsequently promote the activation of transcriptional regulators that drive mitochondrial biogenesis and the expression of thermogenic genes³. The most well-studied thermogenic effector is the UCP1 protein. Even though we observed an upregulated expression of the *Ucp1* gene and downregulated expression in UCP1 protein in HFD mice, this is not unusual as comparable findings have been reported in earlier studies⁴⁰. This opposite phenomenon may be attributed to the complex regulation of gene transcription and protein translation⁴¹. Our findings suggest that WAT browning may serve as a mechanism through which *L. reuteri* ZJ617 or spermidine alleviates MetS. However, given the baseline expression of UCP1 in HFD mice is barely detectable, we acknowledged that the mild browning induced by *L. reuteri* ZJ617 may not completely account for leanness and an

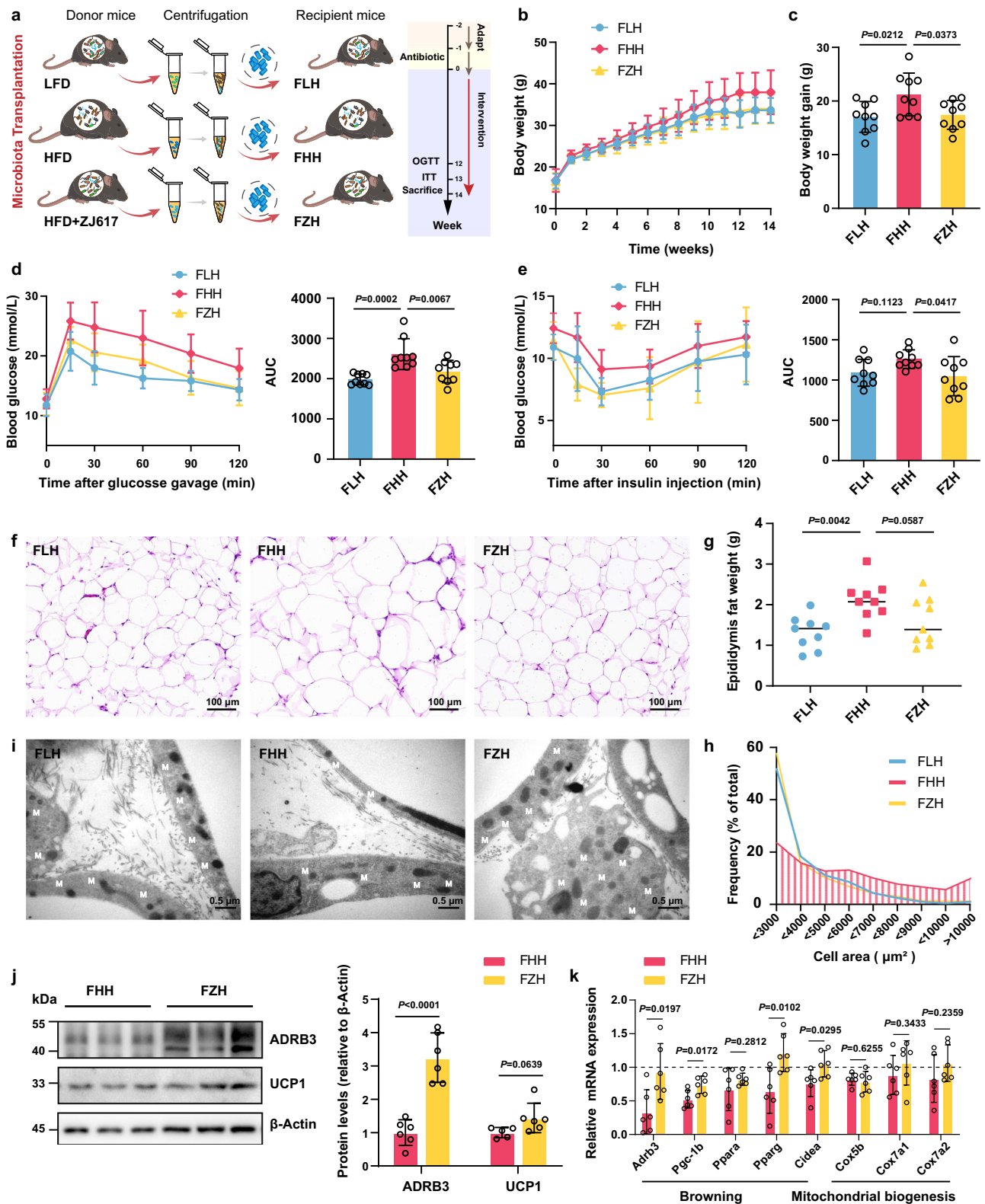
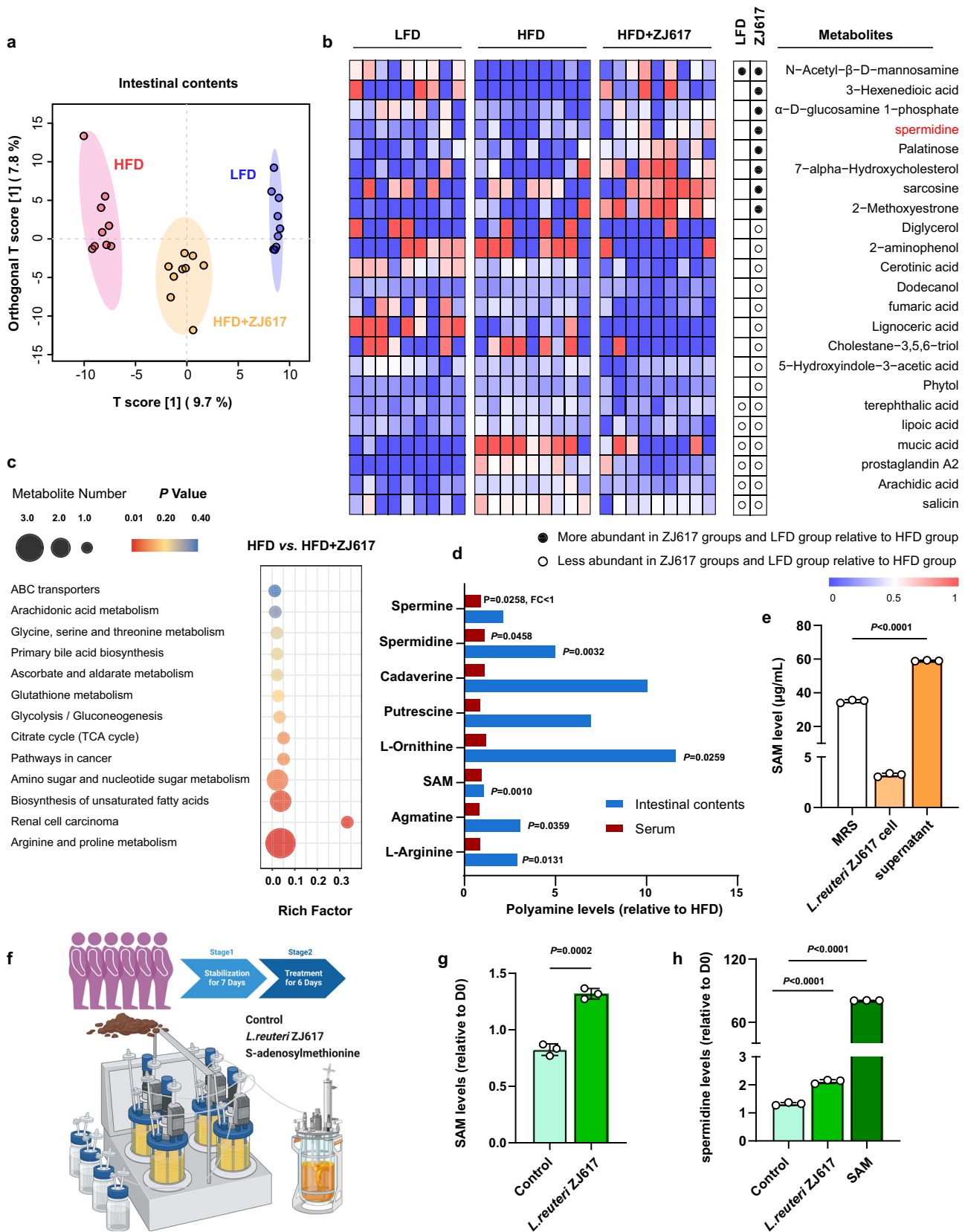


Fig. 4 | Transplantation of *L. reuteri* ZJ617-induced microbiota ameliorates metabolic syndrome in HFD-fed mice. Mice were randomly assigned to three groups and pre-treated with an antibiotic mixture. The fecal microbiota was gavaged into the corresponding group. All mice were maintained on HFD for 14 weeks ($n = 9$ per group). **a** Study design of microbiota transplantation experiment. The figure is drawn by Adobe Illustrator CC 2018. **b** Body weight and **c** body weight gain. **d** Glucose tolerance measured by OGTT. Right: area under the curve (AUC). **e** Insulin tolerance was measured by ITT. Right: area under the curve (AUC). **f** Representative

H&E picture of WAT (scale bars, 100 μm). **g** WAT weight. **h** Frequency distribution of adipocyte cell size. **i** Representative TEM-image of WAT (scale bars, 0.5 μm). **j** Protein levels of ADRB3 and UCP1 in WAT ($n = 6$ per group). **k** mRNA levels of thermogenesis-related genes relative to *Gapdh* in WAT ($n = 6$ per group). FLH group is considered as a reference and represented by a dashed line. Data were shown as mean ± SD. Significances in all panels are calculated based on one-way ANOVA with Dunnett tests for multiple-group comparisons, with the exception of (**j**, **k**) calculated based on two-tailed *t*-tests. Source data are provided as a Source Data file.



improved metabolic phenotype. Therefore, the specific contribution of UCP1 and ADRB3 proteins to the browning process induced by *L. reuteri* ZJ617 and the spermidine remains to be elucidated in further studies. Furthermore, spermidine has been shown to exert a range of beneficial effects on cardiovascular disease protection, lifespan

extension⁴², bone loss prevention⁴³, antitumor immunity⁴⁴, and oocyte quality⁴⁵ improvement. Given these diverse biological roles, the increased spermidine production induced by *L. reuteri* ZJ617 may have broad physiological implications that go well beyond metabolic diseases.

Fig. 5 | *L. reuteri* ZJ617 alters the metabolic profile of HFD-fed mice and increases the production of spermidine. **a** OPLS-DA score plot for discriminating the metabolic profile of the LFD, HFD, and HFD + ZJ617. **b** Heatmaps showing the differential metabolites between HFD and HFD + ZJ617. **c** The metabolic pathways in HFD versus HFD + ZJ617. **d** Fold change of metabolite levels in the polyamine pathway in intestinal contents from mice treated with *L. reuteri* ZJ617 versus the control HFD ($n = 9$ per group). *L. reuteri* ZJ617 was independently cultured three times, and the **(e)** *S*-adenosylmethionine level in both the culture broth and cells were measured ($n = 3$ per group). **f** Study design of in vitro gastrointestinal tract simulation. The figure was created in BioRender. Ma, Y. (2024) <https://BioRender.com/n79v306>.

The feces were collected from six adult volunteers with obesity (BMI ≥ 28). The fecal slurry was prepared and initially stabilized for 7 days, followed by 6 days of continuous fermentation during which *L. reuteri* ZJ617 or *S*-adenosylmethionine (SAM) was added daily. Each sample was collected from three independent fermentation waste extractions. **g** *S*-adenosylmethionine levels in fermentation broth. **h** Spermidine levels in the fermentation broth. Data were shown as mean \pm SD. Significance is calculated based on two-tailed *t*-tests, with the exception of **b** calculated based on two-tailed Wilcoxon tests, **c** calculated based on a two-tailed hypergeometric test. Source data are provided as a Source Data file.

Our study has proven the significance of SAM in mediating microbial spermidine synthesis and the metabolic benefits of *Lactobacillus*. Further studies are needed to generate high-yield SAM-producing *Lactobacillus* strains. Integrating synthetic biology and metabolomics, as previously done to optimize spermidine production in engineered probiotics⁴⁶, could be key to this advancement. These methodologies provide promising strategies for developing probiotic strains with targeted metabolic outputs, facilitating the translation from laboratory-scale research to semi-industrial-scale applications. Additionally, because *L. reuteri* ZJ617 has a regulatory effect on promoting spermidine production in gut microbes from individuals with obesity, clinical experiments are needed to better assess the effects of long-term use of *L. reuteri* ZJ617 on managing metabolic-related diseases.

In summary, our work revealed *L. reuteri* ZJ617 mitigates MetS via promoting spermidine synthesis in the intestine by supplying substrate to spermidine-producing bacteria and preventing those bacteria from declining (Supplementary Fig. 8). Spermidine produced by *L. reuteri* ZJ617 improves MetS are linked to enhance whole-body energy metabolism, activate WAT thermogenesis, and improve insulin resistance. Our work may serve as a foundation for the development of a microbiota-based therapeutic approach to treat MetS in clinics.

Methods

Ethics declarations

All animal experiments were performed in accordance with the “Regulation for the Use of Experimental Animals” of Zhejiang Province, China, and approved by the Animal Care and Use Committee of Zhejiang University (Ethics Code Permit Number: ZJU20170529; ZJU20240770). Fecal samples from healthy volunteers with obesity (BMI ≥ 28) was performed with the approval of the Ethical Committee of The Second Affiliated Hospital of Zhejiang University (Ethics Code Permit Number: 2024-1195). All participants provided written informed consent for sample collection and subsequent experiments.

Animals and *L. reuteri* ZJ617 administration

Four-week-old male, specific pathogen-free (SPF) C57BL/6J mice were obtained from Shanghai SLAC Laboratory Animal Co., Ltd. (Shanghai, China). Before the onset of the experiment, they were acclimatized to the environment (23 ± 1 °C, 12-h light-dark cycle, $50\% \pm 5$ humidity) with free and unlimited access to food and drinking water for one week. Then mice were randomly assigned into three groups (3 cages/group): LFD (Low-fat diet, containing 70% kcal from carbohydrate and 10% kcal from fat (-5.5% kcal from soybean Oil and -4.5% from kcal Lard); PD450J), HFD (High-fat diet, containing 20% kcal from carbohydrate and 60% kcal from fat (-5.5% kcal from soybean Oil and -54.5% kcal from Lard); PD6001) and HFD supplement with *L. reuteri* ZJ617. All diets were from Changzhou SYSE Bio-Tec. Co., Ltd. (Changzhou, China), and the diet composition is given in Supplementary Table 1. The mice were allowed free access to food and were maintained for 14 weeks.

L. reuteri ZJ617 had previously been isolated from piglet small intestines and stored in 20% glycerol at -80 °C until usage. The strain

was anaerobically cultured for 18 h in sterilized De Man Rogosa and Sharpe (MRS) medium at 37 °C. Cultures were collected in the log phase and diluted to 10^9 colony-forming units/mL in drinking water. There was no significant difference in the number of alive *L. reuteri* ZJ617, after placement in water for 24 h. The drinking water was refreshed every day. The abundance of *Lactobacillus* was calculated using plate colony-counting.

Fecal microbiota transplantation

The procedure of fecal microbiota transplantation was done according to a previous study and modified⁴⁷. Feces were collected from the donor LFD, HFD, and HFD + ZJ617 groups, respectively, at the end of week 14, and the pooled sample in each group was used for the following experiment. The fecal pellets were diluted with sterile PBS (100 mg/mL). The mixtures were centrifuged at $1000 \times g$, 4 °C for 5 min. The supernatant was transferred into a new tube and centrifuged for 5 min at $15,000 \times g$ to precipitate the bacteria. Then, the bacterial pellets were resuspended in 600 μ L sterile PBS, and an equal volume of 40% sterile glycerol was added. The resuspended bacteria were stored at -80 °C for later use with transplantation.

Four-week-old male C57BL/6J mice were acclimatized for 1 week, then their intestinal microbiota was first depleted by an antibiotic mixture (vancomycin (0.5 g/L), neomycin sulfate (1 g/L), metronidazole (1 g/L), and ampicillin (1 g/L)) in drinking water for 1 week. Then, the 100 μ L of bacteria suspension was transplanted to the mice that had been pre-treated with antibiotics via oral gavage for 14 weeks (three times per week). All mice were fed the same diet, HFD, for 14 weeks.

Histological analysis

After euthanasia, the liver and adipose tissues of mice were preserved in 4% paraformaldehyde (4% PFA). The fixed paraffin-embedded sample sections were stained with hematoxylin and eosin (H&E) to assess liver steatosis and adipocyte size, respectively, followed by microscopical examination. All processes were performed according to the manufacturer’s instructions. Adipocyte sizes were quantified by Cellpose 2.0 v and ImageJ 1.52 v. The slices were collected and evaluated in a blinded manner.

Transmission electron microscope

Adipose tissues were preserved in 2.5% glutaraldehyde for more than 4 h and then were post-fixed with 1% OsO_4 . The double-fixed Spurr resin-embedded sample sections were stained by uranyl acetate and alkaline lead citrate for 5 min, respectively, and then mitochondria were observed with a TEM (Hitachi Model H-7650). All processes were performed according to the instructions of the Bio-ultrastructure analysis Laboratory of Analysis center of Agrobiological and environmental sciences, Zhejiang University. The slices were collected and evaluated in a blinded manner.

Glucose homeostasis

For oral glucose tolerance testing (OGTT), all mice were placed in clean cages and provided with water but without food. After 6 h of fasting, the mice were administered an oral glucose (2 g/kg, Sigma-Aldrich,

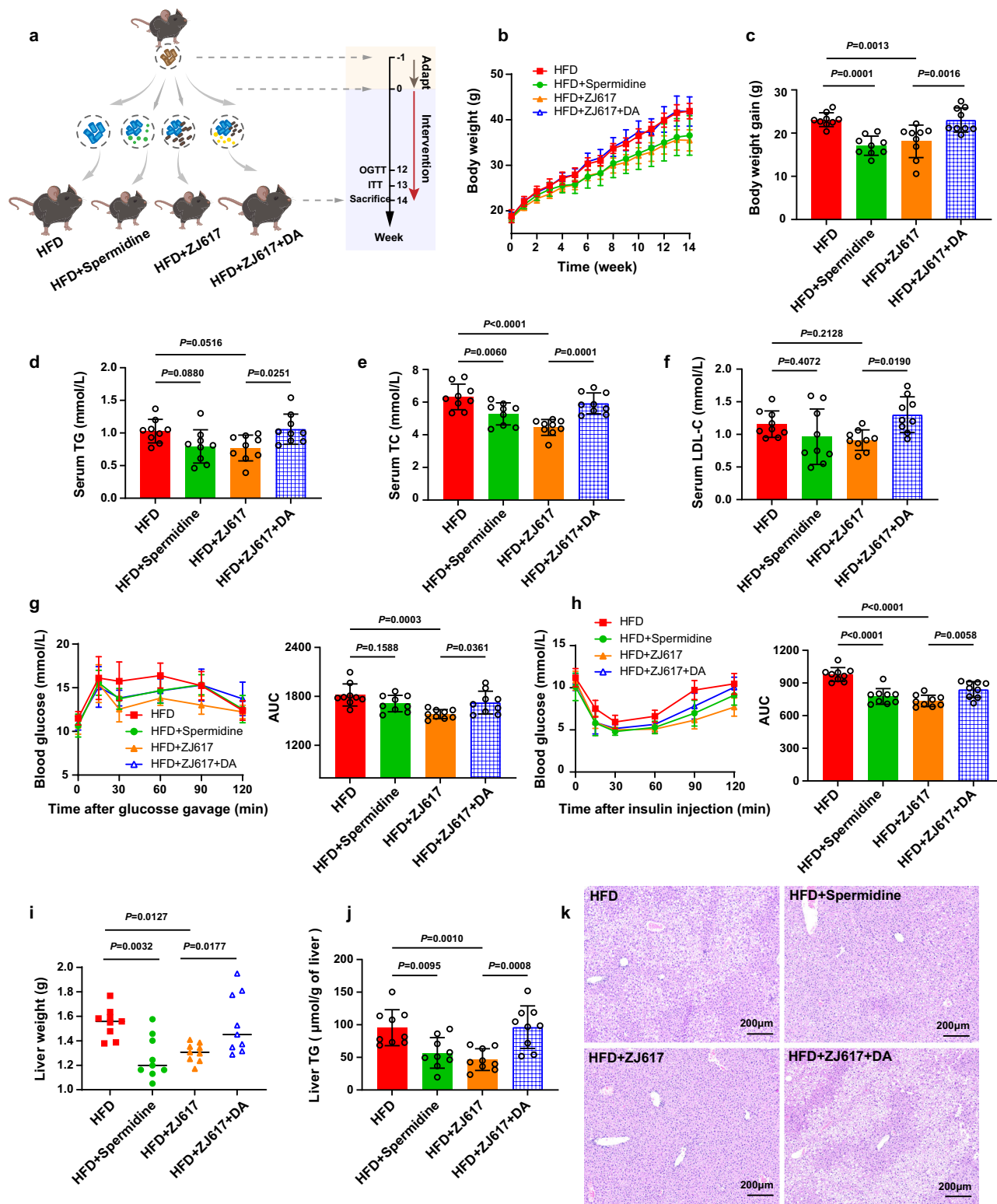


Fig. 6 | Microbial production of spermidine ameliorates MetS in HFD-fed mice. HFD-fed mice were supplemented with freshly prepared drinking water, *L. reuteri* ZJ617 (10^9 CFU/mL) or spermidine (20 mg/kg). Half of the mice were treated on *L. reuteri* ZJ617 were orally gavaged with DA (2.5 mg/kg) every day ($n = 9$ per group). **a** Study design of spermidine supplement experiment. The figure is drawn by Adobe Illustrator CC 2018. **b** Body weights and **c** body weight gains of the above four groups of mice. **d** Triglycerides, **e** Total cholesterol, **f** LDL-C levels in serum.

g Blood glucose tolerance measured by OGTT (left) and AUC (right). **h** Insulin tolerance measured by ITT (left) and AUC (right). **i** Liver weights, **j** Liver triglycerides. **k** Representative H&E pictures of the liver (scale bars, 200 μm). Data were shown as mean \pm SD. Significance is calculated based on one-way ANOVA with Šidák tests for multiple-group comparisons. Source data are provided as a Source Data file.

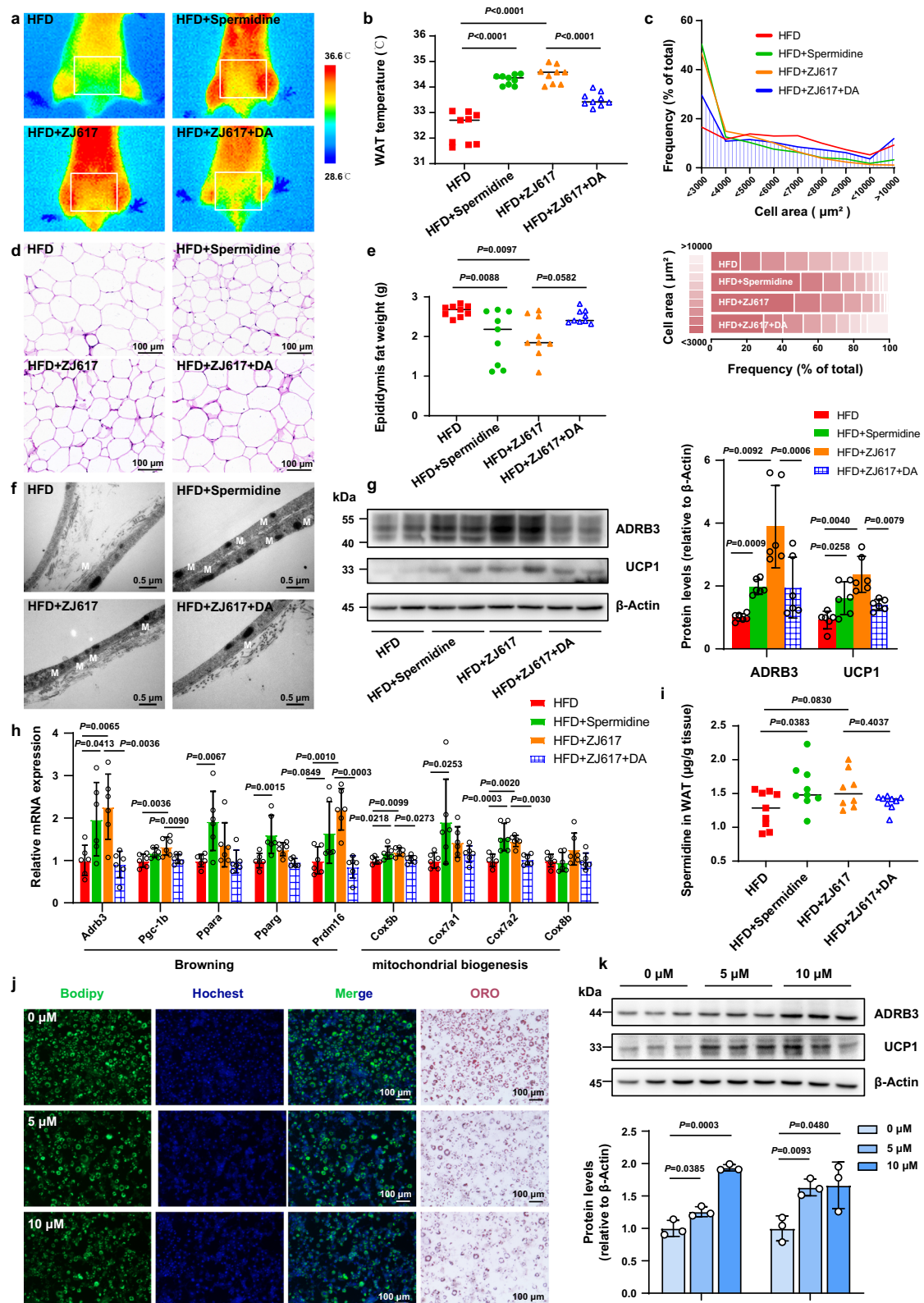


Fig. 7 | Microbiota-derived spermidine promotes browning of mouse white adipose tissue and 3T3-L1 adipocytes. **a** Representative infrared thermal images and **b** the mean temperatures in WAT were measured at the end of the experiment ($n = 9$ per group). **c** Frequency distribution of adipocyte sizes. **d** Representative H&E picture of WAT (scale bars, 100 μm). **e** WAT weights ($n = 9$ per group). **f** Representative TEM images of WAT (scale bars, 0.5 μm). **g** Protein levels of ADRB3 and UCP1 in WAT ($n = 6$ per group). Samples were derived from the same experiment, and gels/blots were processed in parallel. **h** mRNA levels of non-shivering thermogenesis-related genes relative to *Gapdh* in WAT ($n = 6$ biological

replicates per group). **i** Spermidine contents in WAT (HFD, HFD + Spermidine, HFD + ZJ617 + DA, $n = 9$, HFD + ZJ617, $n = 8$). **j** Representative images showing the status of lipid droplets stained with Bodipy 493/503 (green) or Oil red O staining in 3T3-L1 adipocyte (scale bars, 100 μm). **k** Protein levels of ADRB3 and UCP1 in 3T3-L1 adipocyte ($n = 3$ per group). The 3T3-L1 adipocyte was independently cultured three times. Data were shown as mean \pm SD. Significances in all panels are calculated based on one-way ANOVA with Šidák for multiple-group comparisons, with the exception of (**k**) calculated based on two-tailed *t*-tests. Source data are provided as a Source Data file.

158968). Blood glucose levels were measured before and after oral glucose administration at 15, 30, 60, 90, and 120 min and determined with a glucose meter (Accu-Chek Performa, Roche) on blood samples collected from the tip of the tail vein during week 12.

For insulin tolerance testing (ITT), all mice were placed in clean cages and provided with water but no food. After five hours of fasting, the mice were injected with insulin (0.75 U/kg, Sigma-Aldrich, I2643), and blood glucose levels were measured before and after injection at 15, 30, 60, 90, and 120 min after injection during week 13.

Biochemical analysis

Blood samples were centrifuged at $3000 \times g$ for 15 min at 4 °C to produce serum samples. The levels of serum AST, ALT, TG, TC, and LDL-C were determined using the corresponding assay kits (CO10-2-1, CO09-2-1, A110-1-1, A111-1-1, and A113-1-1, respectively; Nanjing Jiancheng Bioengineering Institute, Nanjing, China). Serum insulin levels were measured using ELISA kits (H203-1-1, Nanjing Jiancheng Bioengineering Institute, Nanjing, China). Liver tissues were homogenized with ethanol and centrifuged at $2500 \times g$ for 10 min at 4 °C, and the supernatant was used to determine TG. All indexes were used a multifunctional microplate reader (TECAN, Switzerland), according to the manufacturer's protocols.

Real-time qPCR

Total RNA was extracted using a SteadyPure Universal RNA Extraction kit (Accurate Biotechnology, AG21017, China) according to the manufacturer's protocols. RNA concentrations were equalized and converted to cDNA using a kit (Accurate Biotechnology, AG11728, China). Gene expression was measured by qPCR detection (Bio-Rad, CFX96, USA) systems using SYBR Green (Accurate Biotechnology, AG11701, China). Expression was normalized to glyceraldehyde-3-phosphate dehydrogenase (GAPDH) control. The primer is given in Supplementary Table 2.

Western blot

White adipose tissue and cells were lysed with RIPA buffer containing PMSF, proteinase inhibitor, and phosphatase inhibitors (Beyotime Technology, Shanghai, China) in an ice bath followed by centrifugation at $-13,000 \times g$ for 10 min. The supernatant was collected and denatured in a sample buffer and resolved with SDS-PAGE. Samples were transferred to PVDF membranes with a pore size of 0.45 μm . Individual proteins were detected using 1:1000 dilution of primary antibodies, as follows: ADRB3 (1:1000, Abcam, ab94506, polyclonal antibody), UCPI (1:1000, Abcam, ab234430, polyclonal antibody) and β -actin (1:1000, Cell Signaling Technology, 4970, polyclonal antibody). Proteins were visualized on film with horseradish peroxidase-conjugated secondary antibodies diluted 1:5000.

16S rDNA amplicon sequencing

The V3-V4 region of the bacteria 16S ribosomal RNA genes were amplified using primers 341 F 5'-CCTACGGGGRSGCAGCAG-3' and 806 R 5'-GGACTACVGGGTATCTAATC-3'. PCRs were performed, and the library was constructed using Qubit. The purified amplicons were pooled in equimolar amounts, and paired-end sequenced on an Illumina MiSeq PE250 platform (Study1)/NovaSeq PE250 platform (Study2) (Illumina, San Diego, USA) according to the manufacturer's protocols. ASVs were selected via standard clustering with 100% similarity using Deblur. Each representative tag was assigned to a taxon using the RDP Classifier. The QIIME2 was implemented for ASVs profiling.

PICRUSt2 for prediction of metagenome functions

PICRUSt2 was utilized to predict metagenome functions⁴⁸. Gene banks such as Kyoto Encyclopedia of Genes and Genomes (KEGG

Orthologous, KO), Enzyme Commission numbers (EC no.), and Clusters of Orthologous Groups (COG) were used to support functional gene and pathway profiles. All predicted pathways and differently expressed genes were obtained using a Wilcoxon test.

Metabolomic profiling of intestinal contents

For metabolomic analysis, intestinal contents were collected and immediately snap-frozen in liquid nitrogen. The metabolites were analyzed by gas chromatography time-of-flight mass spectrometer (GC-TOF-MS), according to our previous study⁴⁹. The pre-weighted intestinal contents were extracted and homogenized with a pre-cold mixture (methanol/chloroform, v: v = 3:1). The centrifuged and speed-vacuum-dried metabolites were solubilized in 40 μL of methoxyamination hydrochloride (20 mg/mL in pyridine) and then incubated at 80 °C for 30 min, then derivatized by 60 μL of BSTFA reagent (1% TMCS, v/v) at 80 °C for 1.5 h. The cooled samples were mixed with fatty acid methyl esters (FAMES; 5 μL in chloroform) and injected into the GC-TOF-MS system for detection and analysis.

For the data of the metabolites of intestinal contents, the abundance differences were obtained using a Wilcoxon test. OPLS-DA was conducted to identify the discrimination of variables. Differential metabolites were defined as those with variable importance in the projection (VIP) >1.0 obtained from OPLS-DA and $P < 0.05$.

In vitro gastrointestinal tract simulation

In vitro fecal microbiota fermentation was conducted with a gastrointestinal tract simulation system as described previously with some modification^{50,51}. The feces were collected from six adult volunteers with obesity (BMI ≥ 28 , aged 20–25) who had not taken any antibiotics and probiotics in the past 6 months. The fecal slurry (1:9; w/v) was prepared by diluting the homogenized fecal sample in sterile PBS medium, which was added into the colon simulation bioreactor with nutrient medium (1:9; v/v). After 24 h of inoculation and culture, fresh nutrient medium was added into the bioreactor and waste was drained at a certain rate (Stage 1) to maintain the normal growth of microorganisms. *L. reuteri* ZJ617 (10^9 CFU) and *S*-adenosylmethionine (0.05% w/v; equal to 0.8 g/day for an adult according to previous study⁵²) was added to the reactor. The fermentation lasted for 6 days (Stage 2). During the entire fermentation process, the culture was automatically supplemented with 0.5 mol/L NaOH solution and diluted with HCl to adjust the pH to 6.8. The speed of the stirring rotor was set at 80 r/min. The temperature was kept at 37 °C modulated by the heating and cooling system. Anaerobic conditions were generated by flushing the headspace of all reactions and medium vessels with N_2 for 30 min and three times per day. Each sample was collected from three independent fermentation waste extraction at the beginning and end of stage 2 for spermidine-producing bacteria or spermidine determination.

Bacteroides uniformis

Bacteroides uniformis were obtained from our previous study⁵³. Briefly, the experiment consisted of three groups: medium only (Control), medium supplemented with 10 μM *S*-adenosylmethionine (SAM), and medium supplemented with SAM and *B. uniformis* (*B. uniformis* + SAM). All groups were placed in a vinyl anaerobic chamber (Coy Drive 14,500, USA) and anaerobically cultured at 37 °C for 48 h. At the end of the experiment, all samples were harvested for spermidine determination.

Concentration of spermidine

The concentration of spermidine in intestinal contents, serum, adipose tissue, and bacteria fermentation supernatant was analyzed by UHPLC-MS/MS or HPLC, as previously described and modified⁵⁴. The weighted intestinal contents, serum and adipose tissues and the bacteria fermentation supernatant were extracted and homogenized with ice-cold perchloric acid solution (0.4 mol/L), the bacteria were disrupted by sonication. All samples were derivatized after pH was adjusted to 9.0.

Dansyl chloride acetone solution (10 mg/mL, Aladdin, D13513) was applied for derivatization. Nitrogen-dried metabolites were resububilized in HPLC-grade acetonitrile (Sigma-Aldrich, 34851) and injected into the HPLC system while obtaining spermidine ion traces.

Spermidine supplementation and inhibitor treatment

Four-week-old male C57BL/6j mice were acclimatized for one week. HFD-fed mice were supplemented with spermidine (20 mg/kg) in drinking water for 14 weeks. The dosage was determined based on a previous study³⁵. The drinking water was refreshed every day. The concentration of spermidine in drinking water was adjusted as w/v based on the changes in body weight and water consumption. For the spermidine synthesis inhibitor, HFD-fed mice were supplemented with *L. reuteri* ZJ617 and oral gavage with diminazene aceturate (2.5 mg/kg) daily for 14 weeks. The mice were allowed free access to food and were maintained for 14 weeks.

Metabolic rate measurements

The mouse metabolic rate was assessed after 4 weeks of treatment with *L. reuteri* ZJ617 or 14 weeks of treatment with spermidine, using the TSE PhenoMaster System (TSE PhenoMaster, Germany) following the manufacturer's instructions. Before the metabolic rate was monitored, mice were individually caged for 24 h to acclimate to the system.

Cell culture and staining

The 3T3-L1 preadipocytes (SCSP-5038) were purchased from the National Collection of Authenticated Cell Cultures, grown in high-glucose DMEM (Gibco) supplemented with 10% calf serum (Sigma-Aldrich, B7447) and 1% penicillin-streptomycin at 37 °C in an incubator containing 5% CO₂, followed by feeding with fresh medium every 2 days to reach confluence. For beige adipocyte differentiation, the cells were induced with an induction medium containing DMEM, 10% FBS, 0.5 mM isobutylmethylxanthine, 1 μM dexamethasone, 4.5 μg/mL insulin, and 1 μM rosiglitazone with or without spermidine or PBS for 48 h, and further growth medium was supplemented with insulin with or without spermidine or PBS every 2 days for 6 days. The cultured 3T3-L1 adipocytes were stained using an Oil Red O staining Kit (Solarbio, G1262, China) according to the manufacturer's protocols. The images of the ORO staining were recorded with a microscope and quantified by Image J 1.52v. The images were collected and evaluated in a blinded manner.

Statistics and reproducibility

For assessing differences between the two groups, a two-tailed *t*-test was performed. For differences among more than two groups, a one-way analysis variance (ANOVA) was performed, followed by Dunnett tests (Study1 and Study2) or Šidák tests (Study3). All data are shown as means ± SD. Statistical analyses were performed using GraphPad Prism 9.0v (USA). *P* < 0.05 was considered statistically significant. Results from representative experiments (such as micrographs) were obtained from at least three independent fields of view with similar results.

Reporting summary

Further information on research design is available in the Nature Portfolio Reporting Summary linked to this article.

Data availability

The sequence data from all 16S rRNA sequencing experiments have been deposited in the National Center for Biotechnology Information Sequence Read Archive (SRA) under accession number [PRJNA945511](https://www.ncbi.nlm.nih.gov/sra/PRJNA945511). For the metabolome data have been deposited in the OMIX, China National Center for Bioinformatics, under accession number [OMIX008190](https://www.omics.org.cn/OMIX008190). The genome sequencing and assembly of *Lactobacillus reuteri* ZJ617 have been deposited in the Genome Warehouse in the National Genomics Data Center under accession number

[PRJCA033409](https://www.gwh.org.cn/PRJCA033409). All data supporting the findings of this study are available in the manuscript or Supplementary Data. Source data are provided with this paper.

References

1. McCracken, E., Monaghan, M. & Sreenivasan, S. Pathophysiology of the metabolic syndrome. *Clin. Dermatol.* **36**, 14–20 (2018).
2. Friedman, S. L., Neuschwander-Tetri, B. A., Rinella, M. & Sanyal, A. J. Mechanisms of NAFLD development and therapeutic strategies. *Nat. Med.* **24**, 908–922 (2018).
3. Sakers, A., De Siqueira, M. K., Seale, P. & Villanueva, C. J. Adipose-tissue plasticity in health and disease. *Cell* **185**, 419–446 (2022).
4. Després, J. P. Is visceral obesity the cause of the metabolic syndrome? *Ann. Med.* **38**, 52–63 (2006).
5. Yoneshiro, T. et al. Recruited brown adipose tissue as an antiobesity agent in humans. *J. Clin. Invest.* **123**, 3404–3408 (2013).
6. Yoneshiro, T. et al. Age-related decrease in cold-activated brown adipose tissue and accumulation of body fat in healthy humans. *Obesity* **19**, 1755–1760 (2011).
7. Cohen, P. & Kajimura, S. The cellular and functional complexity of thermogenic fat. *Nat. Rev. Mol. Cell Biol.* **22**, 393–409 (2021).
8. Sanders, M. E., Merenstein, D. J., Reid, G., Gibson, G. R. & Rastall, R. A. Probiotics and prebiotics in intestinal health and disease: from biology to the clinic. *Nat. Rev. Gastroenterol. Hepatol.* **16**, 605–616 (2019).
9. Chen, C. et al. *Prevotella copri* increases fat accumulation in pigs fed with formula diets. *Microbiome* **9**, 175 (2021).
10. Tenorio-Jiménez, C. et al. Evaluation of the effect of *Lactobacillus reuteri* V3401 on biomarkers of inflammation, cardiovascular risk and liver steatosis in obese adults with metabolic syndrome: a randomized clinical trial (PROSIR). *BMC Complement Altern. Med.* **18**, 306 (2018).
11. Tenorio-Jiménez, C. et al. *Lactobacillus reuteri* V3401 reduces inflammatory biomarkers and modifies the gastrointestinal microbiome in adults with metabolic syndrome: the PROSIR study. *Nutrients* **11**, 1761 (2019).
12. Simon, M. C. et al. Intake of *Lactobacillus reuteri* improves incretin and insulin secretion in glucose-tolerant humans: a proof of concept. *Diabetes Care* **38**, 1827–1834 (2015).
13. Chen, L. H. et al. Antiobesity effect of *Lactobacillus reuteri* 263 associated with energy metabolism remodeling of white adipose tissue in high-energy-diet-fed rats. *J. Nutr. Biochem.* **54**, 87–94 (2018).
14. Fan, Y. & Pedersen, O. Gut microbiota in human metabolic health and disease. *Nat. Rev. Microbiol.* **19**, 55–71 (2021).
15. Cani, P. D. et al. Microbial regulation of organismal energy homeostasis. *Nat. Metab.* **1**, 34–46 (2019).
16. Wang, D. et al. LSD1 mediates microbial metabolite butyrate-induced thermogenesis in brown and white adipose tissue. *Metabolism* **102**, 154011 (2020).
17. Kang, Y. et al. *Lactobacillus acidophilus* ameliorates obesity in mice through modulation of gut microbiota dysbiosis and intestinal permeability. *Pharmacol. Res.* **175**, 106020 (2022).
18. Zhu, T. et al. *L. reuteri* ZJ617 inhibits inflammatory and autophagy signaling pathways in gut-liver axis in piglet induced by lipopolysaccharide. *J. Anim. Sci. Biotechnol.* **12**, 110 (2021).
19. Cui, Y. et al. *Lactobacillus reuteri* ZJ617 culture supernatant attenuates acute liver injury induced in mice by lipopolysaccharide. *J. Nutr.* **149**, 2046–2055 (2019).
20. Gao, K. et al. Doses *Lactobacillus reuteri* depend on adhesive ability to modulate the intestinal immune response and metabolism in mice challenged with lipopolysaccharide. *Sci. Rep.* **6**, 28332 (2016).
21. Wang, J. et al. Modulation of gut microbiota during probiotic-mediated attenuation of metabolic syndrome in high fat diet-fed mice. *ISME J.* **9**, 1–15 (2015).

22. Hamana, K., Itoh, T., Benno, Y. & Hayashi, H. Polyamine distribution profiles of new members of the phylum Bacteroidetes. *J. Gen. Appl. Microbiol.* **54**, 229–236 (2008).
23. Sugiyama, Y. et al. Comprehensive analysis of polyamine transport and biosynthesis in the dominant human gut bacteria: potential presence of novel polyamine metabolism and transport genes. *Int. J. Biochem. Cell Biol.* **93**, 52–61 (2017).
24. Madeo, F., Eisenberg, T., Pietroccola, F. & Kroemer, G. Spermidine in health and disease. *Science* **359**, eaan2788 (2018).
25. Karvonen, E., Kauppinen, L., Partanen, T. & Pösö, H. Irreversible inhibition of putrescine-stimulated S-adenosyl-L-methionine decarboxylase by berenil and pentamidine. *Biochem. J.* **231**, 165–169 (1985).
26. Mukhopadhyay, R. & Madhubala, R. Antileishmanial activity of berenil and methylglyoxal bis (guanylhydrazone) and its correlation with S-adenosylmethionine decarboxylase and polyamines. *Int. J. Biochem. Cell Biol.* **27**, 55–59 (1995).
27. Neidhart, M., Karouzakis, E., Jüngel, A., Gay, R. E. & Gay, S. Inhibition of spermidine/spermine N1-acetyltransferase activity: a new therapeutic concept in rheumatoid arthritis. *Arthritis Rheumatol.* **66**, 1723–1733 (2014).
28. Lewandowski, N. M. et al. Polyamine pathway contributes to the pathogenesis of Parkinson disease. *Proc. Natl Acad. Sci. USA* **107**, 16970–16975 (2010).
29. Zou, D. et al. A comprehensive review of spermidine: safety, health effects, absorption and metabolism, food materials evaluation, physical and chemical processing, and bioprocessing. *Compr. Rev. Food Sci. Food Saf.* **21**, 2820–2842 (2022).
30. Wu, Y., Zhang, Q., Ren, Y. & Ruan, Z. Effect of probiotic *Lactobacillus* on lipid profile: a systematic review and meta-analysis of randomized, controlled trials. *PLoS ONE* **12**, e0178868 (2017).
31. Cui, Y. et al. *Lactobacillus reuteri* ZJ617 maintains intestinal integrity via regulating tight junction, autophagy and apoptosis in mice challenged with lipopolysaccharide. *Oncotarget* **8**, 77489–77499 (2017).
32. Wang, G. et al. *Lactobacillus reuteri* ameliorates intestinal inflammation and modulates gut microbiota and metabolic disorders in dextran sulfate sodium-induced colitis in mice. *Nutrients* **12**, 2298 (2020).
33. Yang, B. et al. *Lactobacillus reuteri* FYNLJ109L1 attenuating metabolic syndrome in mice via gut microbiota modulation and alleviating inflammation. *Foods* **10**, 2081 (2021).
34. Fuchs, R. T., Grundy, F. J. & Henkin, T. M. The S(MK) box is a new SAM-binding RNA for translational regulation of SAM synthetase. *Nat. Struct. Mol. Biol.* **13**, 226–233 (2006).
35. Ma, L. et al. Spermidine improves gut barrier integrity and gut microbiota function in diet-induced obese mice. *Gut Microbes* **12**, 1–19 (2020).
36. Zhou, J. et al. Spermidine-mediated hypusination of translation factor EIF5A improves mitochondrial fatty acid oxidation and prevents non-alcoholic steatohepatitis progression. *Nat. Commun.* **13**, 5202 (2022).
37. Wang, D. et al. Oral spermidine targets brown fat and skeletal muscle to mitigate diet-induced obesity and metabolic disorders. *Mol. Nutr. Food Res.* **65**, e2100315 (2021).
38. Guilherme, A., Virbasius, J. V., Puri, V. & Czech, M. P. Adipocyte dysfunctions linking obesity to insulin resistance and type 2 diabetes. *Nat. Rev. Mol. Cell Biol.* **9**, 367–377 (2008).
39. Monelli, E. et al. Angiocrine polyamine production regulates adiposity. *Nat. Metab.* **4**, 327–343 (2022).
40. López-Almela, I. et al. *Bacteroides uniformis* combined with fiber amplifies metabolic and immune benefits in obese mice. *Gut Microbes* **13**, 1–20 (2021).
41. Liu, Y., Beyer, A. & Aebersold, R. On the dependency of cellular protein levels on mRNA abundance. *Cell* **165**, 535–550 (2016).
42. Eisenberg, T. et al. Cardioprotection and lifespan extension by the natural polyamine spermidine. *Nat. Med.* **22**, 1428–1438 (2016).
43. Yamamoto, T. et al. The natural polyamines spermidine and spermine prevent bone loss through preferential disruption of osteoclastic activation in ovariectomized mice. *Br. J. Pharmacol.* **166**, 1084–1096 (2012).
44. Al-Habsi, M. et al. Spermidine activates mitochondrial trifunctional protein and improves antitumor immunity in mice. *Science* **378**, eabj3510 (2022).
45. Zhang, Y. et al. Polyamine metabolite spermidine rejuvenates oocyte quality by enhancing mitophagy during female reproductive aging. *Nat. Aging* **3**, 1372–1386 (2023).
46. Caffaratti, C., Plazy, C., Cunin, V., Toussaint, B. & Le Gouellec, A. Bioengineering of *Escherichia coli* Nissle 1917 for production and excretion of spermidine, a key metabolite in human health. *Metabolites* **12**, 1061(2022).
47. Wu, T. R. et al. Gut commensal *Parabacteroides goldsteinii* plays a predominant role in the anti-obesity effects of polysaccharides isolated from *Hirsutella sinensis*. *Gut* **68**, 248–262 (2019).
48. Douglas, G. M. et al. PICRUSt2 for prediction of metagenome functions. *Nat. Biotechnol.* **38**, 685–688 (2020).
49. Tang, W. et al. Impairment of intestinal barrier function induced by early weaning via autophagy and apoptosis associated with gut microbiome and metabolites. *Front. Immunol.* **12**, 804870 (2021).
50. Xiang, S. et al. Xylitol enhances synthesis of propionate in the colon via cross-feeding of gut microbiota. *Microbiome* **9**, 62 (2021).
51. Xu, Y. et al. Cobalamin (Vitamin B12) induced a shift in microbial composition and metabolic activity in an in vitro colon simulation. *Front. Microbiol.* **9**, 2780 (2018).
52. Thompson, M. A. et al. Dietary supplement S-adenosyl-L-methionine (AdoMet) effects on plasma homocysteine levels in healthy human subjects: a double-blind, placebo-controlled, randomized clinical trial. *J. Altern. Complement. Med.* **15**, 523–529 (2009).
53. Tang, W. et al. IgA-mediated control of host-microbial interaction during weaning reaction influences gut inflammation. *Gut Microbes* **16**, 2323220 (2024).
54. Galitsopoulou, A., Michaelidou, A. M., Menexes, G. & Alichanidis, E. Polyamine profile in ovine and caprine colostrum and milk. *Food Chem.* **173**, 80–85 (2015).

Acknowledgements

We thank Ms. Junhong Wang and Dr. Weiren Dong from the lab platform of the College of Animal Sciences, Zhejiang University, for their excellent technical guidance and assistance. We specially thank Dr. Huiqing Yu and professor Guangxu Meng from Institute of Immunity and Infection, Chinese Academy of Sciences for kindly providing the TSE Phe-noMaster System and technical support, and professor Xuan Zhu from School of Food Science and Biotechnology, Zhejiang Gongshang University for kindly providing the Gastrointestinal Tract Simulation System. This study was supported by grants from the National Key R&D Program of China (2022YFD1300602), the Key R&D Projects of Zhejiang Province (2023C02026), both awarded by H.W.

Author contributions

Y.M. and H.W. planned the project and the experiments. Y.M., H.W., Y.W., and Y.Z. analyzed the data; Y.M., W.T., J.L., Z.D., J.M., D.L., and S.W. performed the experiments; Y.M. and H.W. wrote the original draft; Y.M., Y.W., H.W., and T.G.V. were responsible for writing review and editing. Funding acquisition was the responsibility of H.W.

Competing interests

The authors declare no competing interests.

Additional information

Supplementary information The online version contains supplementary material available at <https://doi.org/10.1038/s41467-025-56105-4>.

Correspondence and requests for materials should be addressed to Yuhao Wang or Haifeng Wang.

Peer review information *Nature Communications* thanks the anonymous reviewer(s) for their contribution to the peer review of this work. A peer review file is available.

Reprints and permissions information is available at <http://www.nature.com/reprints>

Publisher's note Springer Nature remains neutral with regard to jurisdictional claims in published maps and institutional affiliations.

Open Access This article is licensed under a Creative Commons Attribution-NonCommercial-NoDerivatives 4.0 International License, which permits any non-commercial use, sharing, distribution and reproduction in any medium or format, as long as you give appropriate credit to the original author(s) and the source, provide a link to the Creative Commons licence, and indicate if you modified the licensed material. You do not have permission under this licence to share adapted material derived from this article or parts of it. The images or other third party material in this article are included in the article's Creative Commons licence, unless indicated otherwise in a credit line to the material. If material is not included in the article's Creative Commons licence and your intended use is not permitted by statutory regulation or exceeds the permitted use, you will need to obtain permission directly from the copyright holder. To view a copy of this licence, visit <http://creativecommons.org/licenses/by-nc-nd/4.0/>.

© The Author(s) 2025